AGU PUBLICATIONS

JGR

Journal of Geophysical Research: Oceans

RESEARCH ARTICLE

10.1002/2013JC009642

Key Points:
- SSH peaks at a certain frequency at each latitudinal band
- The linear wave near critical frequency causes the SSH peaks in low latitudes
- Eddies play a more important role in SSH variability in high latitudes

Correspondence to:
X. Lin,
linxiaop@ouc.edu.cn

Citation:
Lin, X., Y. Yin, and J. Yang (2014), A mechanism for the latitudinal dependence of peak-spectrum sea surface height variability, *J. Geophys. Res. Oceans*, *119*, 1431–1444, doi:10.1002/2013JC009642.

Received 21 NOV 2013
Accepted 3 FEB 2014
Accepted article online 12 FEB 2014
Published online 25 FEB 2014

A mechanism for the latitudinal dependence of peak-spectrum sea surface height variability

Xiaopei Lin[1,2,3], Yuqi Yin[1], and Jiayan Yang[3]

[1]Physical Oceanography Laboratory, Ocean University of China, Qingdao, China, [2]Qingdao Colobrative Innovation Center of Marine Science and Technology, Qingdao, China, [3]Department of Physical Oceanography, Woods Hole Oceanographic Institution, Woods Hole, Massachusetts, USA

Abstract Previous studies have shown that the power spectrum of satellite-observed sea surface height (SSH) variability peaks at a certain frequency (or a wave number) band at a given latitude. Lin et al. (2008) attributed this latitudinal dependence to the critical frequency of the first baroclinic mode Rossby waves in the tropical and subtropical oceans. Their study was based on the linear Rossby wave theory and focused on SSH variability in the tropical and subtropical oceans since the altimetry data do not adequately resolve lengths of baroclinic Rossby waves at and near the critical frequency in high latitudes. In this study, we expand their analysis to high-latitude oceanic basins and to include nonlinear eddy effects, by using a linear wave model and a high-resolution model output from the OGCM for the Earth Simulator (OFES). It is found that the linear wave mechanism by and large remains valid in the tropical and subtropical oceans. In higher latitudes as well as in some regions in the western tropical and subtropical oceans, other mechanisms, like nonlinear eddy, play more important role in determining the SSH variability.

1. Introduction

The continuous and nearly global satellite observations of sea surface height (SSH) since 1992 have revealed some important and interesting spectral and spatial patterns of sea level variability [*Qiu et al.*, 1997; *Stammer*, 1997; *Fu and Chelton*, 2001]. With its global coverage, the altimetry data have been used to examine regional SSH variances in both frequency and wave number domains. For instance, *Polito and Liu* [2003] analyzed the TOPEX/Poseidon altimetry data between 1992 and 2000 and found that the SSH variance along 20°N and 20°S in all three basins seemed to peak at the same period of about 3 months. This 3 month variability along 20°N was also reported in other analyses of satellite data [*Liu and Wang*, 1999; *Hu and Liu*, 2002; *Pan et al.*, 2002; *Chen et al.*, 2003] and of tide gauge and current meter records [*Mitchum*, 1995; *Zhang et al.*, 2001; *Lin et al.*, 2004]. *Qiao et al.* [2004] examined high-frequency (with a period shorter than 150 days) SSH variability in the area between 40°S and 40°N and found that its spectrum peaks at a frequency that depends almost solely on the latitudinal position. *Lin et al.* [2008, hereafter LIN08] revisited this topic by analyzing a 14 year data set from 1992 to 2006 and reaffirmed the previous finding that at any latitude there is a period band at which SSH variability has a maximum spectrum (they defined it as the "peak spectrum"). More importantly, they offered a dynamical explanation for this distribution of the peak-spectrum period band. They attributed this latitudinal dependence to linear Rossby wave's critical frequency—a frequency at which the group velocity is zero. Rossby waves are the leading mechanism for redistributing energy flux from the atmosphere. LIN08 argued that the energy of Rossby waves is accumulated in the interior ocean near the critical frequency when the group velocity is zero. Consequently, the spectrum of SSH variability peaks at such a frequency (period) band.

There are several issues that require further investigations. First, the LIN08 study was based purely on spectrum analyses of SSH data. It is still possible that the good correspondence between the peak-spectrum frequency and the critical Rossby-wave frequency is coincidental. In this study, we will further examine the LIN08 mechanism by testing its consistency with the dispersion relation of linear Rossby waves. A one layer reduced gravity model will be used. Second, the critical wavelength, i.e., the wavelength at the critical frequency, decreases poleward. The altimetry observations are insufficient in spatial resolution to resolve such waves in high latitudes as pointed out by LIN08. It remains uncertain whether the LIN08 mechanism is still applicable in high latitudes. Third, recent studies [*Hughes and Williams*, 2010; *Chelton et al.*, 2011] suggested

that nonlinear eddies, rather than linear waves, are more dominant in SSH variability. To address above issues, in this study, we will expand our analyses to higher latitudes and to include eddy effects by using the outputs from the high-resolution OGCM for Earth Simulator (OFES).

The paper is organized as follows: The mechanism proposed by LIN08 will be discussed in the next section. In section 3, we will present the analyses of dynamics and linear wave modeling results. This will be followed by the OFES data set analyses in section 4. A summary is given in section 5.

2. The Critical Frequency of Rossby Waves and Spectrum Peaks of SSH Variability

In this section, we will first review and then examine in more detail the mechanism proposed by LIN08. For a stratified ocean, one can decompose a Rossby wave into a series of vertical modes [*Lighthill*, 1969; *Flierl*, 1978] with the first baroclinic mode being the most dominant internal mode [*Polito and Liu*, 2003]. The frequency and wave number of a free Rossby wave are related through the dispersion relation. There are two distinct classes of Rossby waves. The energy of long waves, i.e., longer than the Rossby deformation radius, propagates westward, while the energy of short ones goes eastward. The phase of either type of waves travels westward. Long Rossby waves are nondispersive, and play the most important role, by far, in oceanic adjustments to changes in atmospheric forcing.

The linear dispersion relation for a first baroclinic mode Rossby wave can be expressed as (see *Pedlosky* [1987] for a more detailed discussion]

$$\omega = \frac{\beta k}{k^2 + l^2 + \left(\frac{1}{d}\right)^2} \tag{1}$$

where $\beta = 2\Omega\cos\theta/R$ (Ω and R are the rotation rate and the radius of the earth, respectively, θ is the latitude, where a Rossby wave propagates) is the meridional gradient of planetary vorticity f and $(k, l) = \frac{2\pi}{(L_\phi, L_\theta)}$ are the wave numbers (L_ϕ and L_θ are the zonal and meridional wave lengths). An important spatial scale in equation (1) is $d = c_1/f$, the Rossby deformation radius, where c_1 is the speed of the first baroclinic long-gravity wave, and is determined by the stratification and depth of the water column and $f = 2\Omega\sin\theta$. A Rossby wave's energy is propagated by its group velocity defined as

$$\begin{aligned} C_{gx} &= \frac{\partial\omega}{\partial k} = \beta\frac{(k^2 - l^2 - d^{-2})}{(k^2 + l^2 + d^{-2})^2} \\ C_{gy} &= \frac{\partial\omega}{\partial l} = \beta\frac{2kl}{(k^2 + l^2 + d^{-2})^2} \end{aligned} \tag{2}$$

For short waves, the energy would propagate meridionally between the equator and the turning latitude (to be discussed later). Here we concentrate on those waves whose meridional group velocities are small and their energy fluxes are mainly zonal. For those waves, their zonal group velocity becomes zero when $l = 0$ and $k = -1/d$. The corresponding frequency (critical frequency) becomes

$$\omega_c = -\frac{\beta d}{2} = -\frac{\beta c_1}{2f} \tag{3}$$

The zonal wave length at this critical frequency becomes

$$L_c = -\frac{2\pi c_1}{f} \tag{4}$$

Both the critical frequency and its associated critical wave length depend on the latitude θ (through f and β), and the hydrographic and bathymetric conditions that determine c_1. The ω_c is also the maximum frequency that a free linear Rossby wave can exist at a given latitude θ for a given c_1. One can also define the critical latitude through (3)

$$\theta_c = \cot^{-1}\left(\frac{2R\omega}{c_1}\right) \tag{5}$$

θ_c is also referred as the turning latitude since poleward propagating Rossby waves would have to turn from this latitude back toward the equator [*Polito and Cornillon*, 1997; *Glazman and Weichman*, 2005].

For a given frequency, the zonal group velocity of a free Rossby wave becomes zero at the critical latitude. This latitude moves poleward with a decreasing frequency as shown by (5). The essence of the LIN08 mechanism is that the ocean responds to an atmospheric forcing has a wide range of frequency. But along any latitude there is a critical frequency at which the first baroclinic mode Rossby wave's energy does not propagate and thus accumulates locally in the ocean interior. This leads to a peak of power spectrum of SSH variability. As noted in the discussion above, short Rossby waves can propagate meridionally within the area bounded by the turning latitude. But such short waves do not prevent the energy accumulation of long waves at the critical frequency.

3. Linear Model Experiments

The LIN08 mechanism was postulated based on spectrum analyses of altimetry data. It needs to be tested in the context of Rossby wave dynamics. A main aspect of the Rossby wave mechanism is that the peak-spectrum distribution is determined mainly by dynamical parameters that govern Rossby wave characteristics rather than by the spatial and temporal variability in the atmospheric forcing fields. This will be tested here by using a simple model, a linear one-layer reduced-gravity model, used by *Yang and Joyce* [2006, here after RG model]. One neat aspect of such a simple model is that the only tunable parameter relevant to Rossby waves is the deformation radius, $d = c_1/f$, in the dispersion relation (1). In the following experiments, we will vary d while keeping the wind-stress forcing unchanged and examine whether the distribution of the peak-spectrum frequency would change according to what would be predicted by the Rossby wave's critical latitude, i.e., (5). The governing equations of the RG model are

$$\begin{aligned}
&\frac{\partial u}{\partial t} - fv + g'\frac{\partial h}{\partial x} = \frac{\tau_x}{\rho H_1} + A_H\nabla^2 u \\
&\frac{\partial v}{\partial t} + fu + g'\frac{\partial h}{\partial y} = \frac{\tau_y}{\rho H_1} + A_H\nabla^2 v \\
&\frac{\partial h}{\partial t} + H_1\left(\frac{\partial u}{\partial x} + \frac{\partial v}{\partial y}\right) = 0
\end{aligned} \tag{6}$$

where h is the deviation of the layer thickness, $g' = (\rho_2 - \rho_1)g/\rho$ is the reduced gravity determined by the density difference between the first and second layers, $\tau_{x,y}$ is wind stress, and $A_H = 35\ \mathrm{m^2\ s^{-1}}$ is the horizontal viscosity. The averaged first layer thickness H_1 is set to be 750 m and the second layer depth is infinity. The model domain extends zonally across the whole Pacific Ocean and meridionally from 45°S to 45°N with a 1/4° spatial resolution. Each boundary is treated as a solid one along which no-normal flow and nonslip conditions are applied. In all numerical experiments, the model is forced by the QuikSCAT wind stress observed by satellite scatterometers [*Liu*, 2002]. The model is spun up for 25 years by using climatology compiled wind stress from an 8 year, 1999–2007, data set. After reaching a quasiequilibrium state, we restart the model by forcing it with a daily wind stress from 1999 to 2007. The output from this latter 8 year simulation is used in our analysis.

In the first experiment (EXP1), we set the density of the first layer $\rho_1 = 1023\ \mathrm{kg\ m^{-3}}$ and the density of the second layer $\rho_2 = 1025\ \mathrm{kg\ m^{-3}}$. This gives the Kelvin wave speed $c_1 = \sqrt{H_1 g'} = 3.6\mathrm{ms}^{-1}$. Following LIN08s procedure, we use the Fast Fourier Transformation (FFT) [*Cooley and Tukey*, 1965] to calculate the power spectrum at every grid point. We repeated the same analysis and integrated the fractional variance into five period bands as LIN08: (a) 15–45 days, (b) 45–75 days, (c) 75–105 days, (d) 105–135 days, and (e) 135–165 days. We should note here that to compare with LIN08, we are effectively considering the spectral power distribution function (SPD—a function of period) rather than a more commonly used power spectral density (PSD—a function of frequency). The curve in SPD is not the same as it is in PSD, with change in slope. But our analysis (figures not shown here) indicates that both SPD and PSD of SSH variability around critical period and critical frequency always show a peak. Figure 1 shows the fractional variance for each of the five

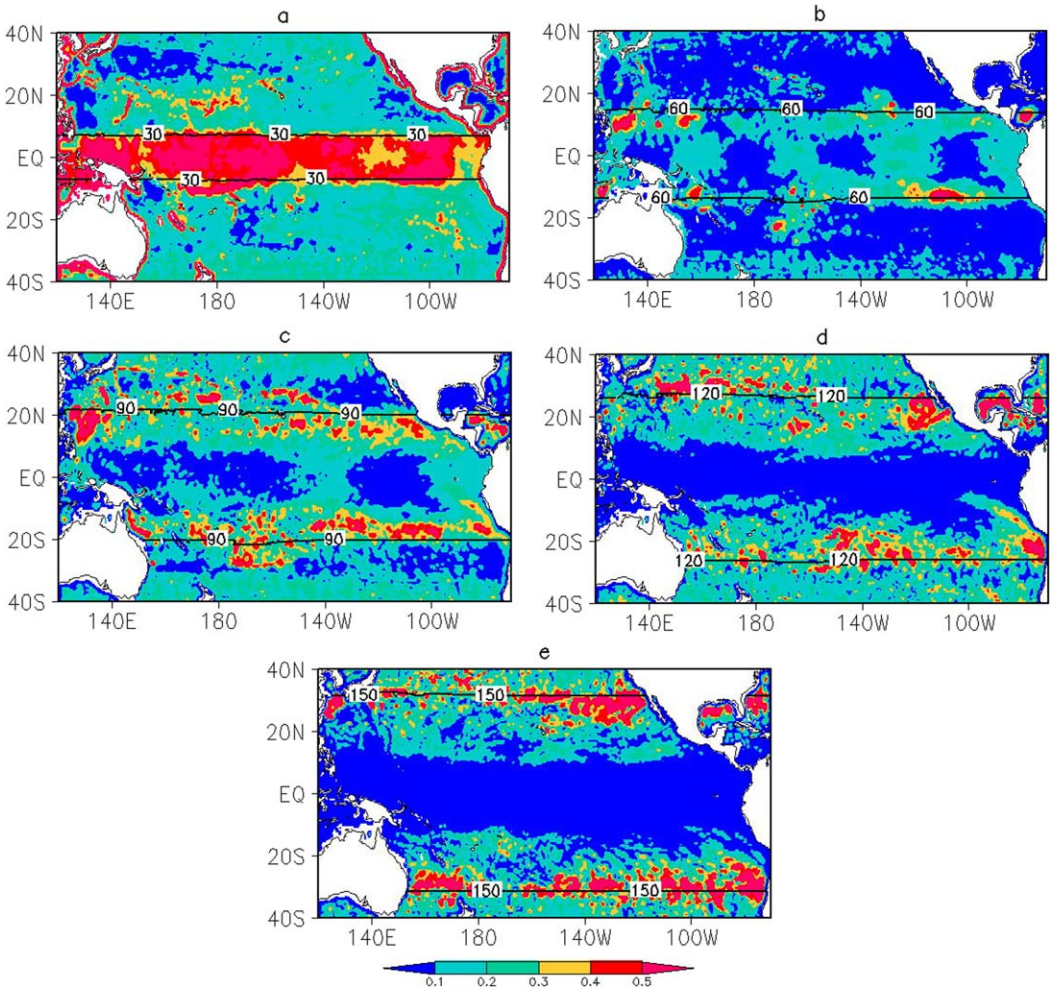

Figure 1. The fractional variance (color shading) between a selected period band and the accumulated one for the period <165 days. The selected frequency band is: (a) $2\pi/15$–$2\pi/45$ days, (b) $2\pi/45$–$2\pi/75$ days, (c) $2\pi/75$–$2\pi/105$ days, (d) $2\pi/105$–$2\pi/135$ days, and (e) $2\pi/135$–$2\pi/165$ days. The SSH data are from EXP1 which used the linear RG model described in equation (6). The theoretically expected critical latitudes (black lines) are computed by equation (5) with $c_1 = 3.6$ m s^{-1} (the value used in EXP1). The results from the simple model are similar to that from a 3-D model shown in Figure 5, and to that from observed altimetry data shown by LIN08.

period bands to the total high-frequency variability (period <165 days) in the global ocean from 40°S to 40°N. Like that in LIN08, the modeled SSH has a similar zonal band distribution of peak-spectrum period (frequency). The black lines in Figure 1 indicate the position of the critical latitude θ_c calculated from the model c_1 for a frequency of $2\pi/30$ days (Figure 1a), $2\pi/60$ days (Figure 1b), $2\pi/90$ days (Figure 1c), $2\pi/120$ days (Figure 1d), and $2\pi/150$ days (Figure 1e). Isolines of θ_c also match well with the latitudinal bands of the peak-spectrum periods for all five selected period ranges.

For a linear Rossby wave, its critical wave number and frequency are related through the dispersion relation. So our argument that Rossby waves at zero group velocity are responsible for peaks in the SSH spectrum would be strengthened if the SSH spectrum would also peak at the critical wave number (or wave length). We applied the two-dimensional FFT (zonal direction and time) to model SSH data in each latitudinal band. Figures 2a and 2b are the power spectrum in wave length-latitude and period-latitude space. The solid lines in Figure 2 are the corresponding critical wave length and critical period that were calculated by using c_1 derived from model parameters. The white lines in Figure 2 indicate the peak-spectrum wave length or wave period. These two curves are basically in accordance with each other. We should point out here that, both in the altimetry data (Figure 3a in LIN08) and in the linear model results (Figure 2a), the consistency with the dispersion relation is always better in the period domain than that in the wave length domain. For

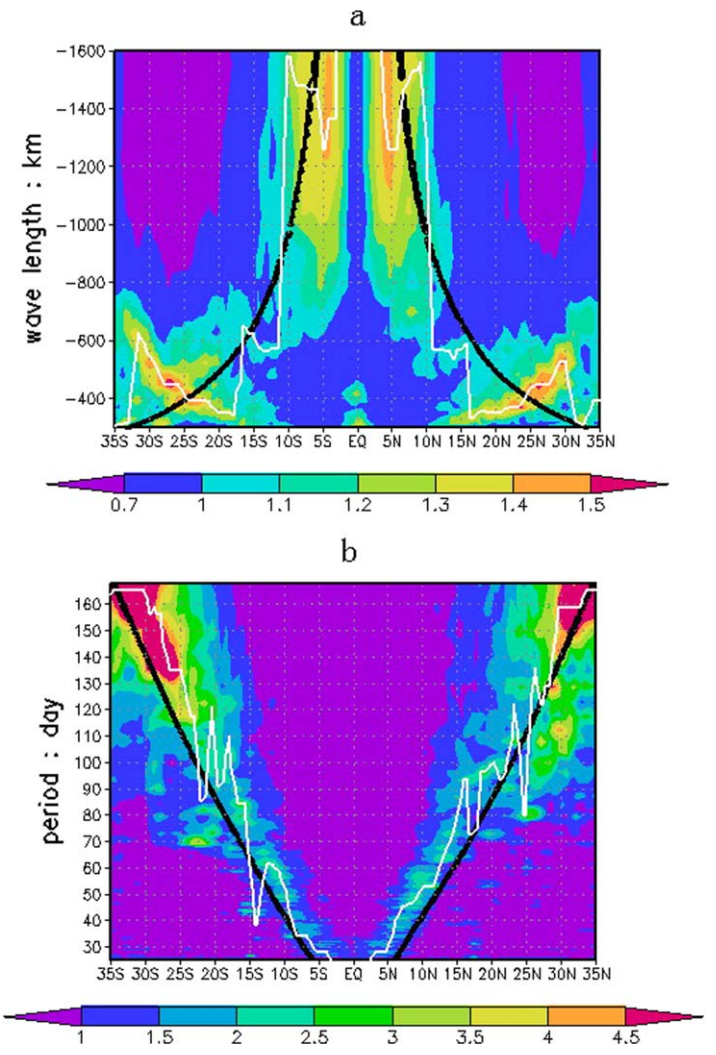

Figure 2. (a) The wave length-latitude energy spectrum and (b) period-latitude energy spectrum from linear model SSH data (color shading). The black lines are the theoretically expected critical wave length and the critical period. The white lines are the most energetic wave length and the period. We notice that there are some discrepancies between the modeled peak-spectrum wave length with the critical wave length. But the results from the simple model are similar to that of a 3-D model shown in Figure 5 and to that from observed altimetry data shown by LIN08. This makes us more confident in applying the model for sensitivity tests (EXP2 and EXP3).

$c_1 = 3.6$ m s^{-1}, the deformation radius is smaller than 50 km at 30°N. So the critical wavelength is not well resolved in the model. The critical period, however, is much better resolved. Furthermore, the LIN08 mechanism is based on the free wave theory while the atmospheric forcing may induce some forced waves in the ocean [*Qiu et al.*, 1997; *White et al.*, 1998] and destroy the consistency. This difference in the spatial and temporal representations of stagnant Rossby waves is probably a cause for the difference of data-theory consistency shown in Figure 2.

In the following experiments, we will use the model to test the consistency between the LIN08 mechanism and the dispersion relation. The only free parameter in both the dispersion relation and the model is c_1 that determines the deformation radius c_1/f. The critical latitude of linear Rossby waves moves poleward (equatorward) when c_1 increases (decreases). The long-gravity wave speed c_1 is determined by the background of ocean stratification. We can modify c_1 in the model either by altering $\Delta\rho$ or by changing the upper layer thickness H_1. In the second experiment (EXP2), we set $\rho_1 = 1024$ kg m^{-3} and the averaged c_1 is reduced to 2.5 m s^{-1} from 3.6 m s^{-1} in EXP1. In the third experiment (EXP3), we set $\rho_1 = 1021$ kg m^{-3} and c_1 increases to 5.1 m s^{-1}. Figures 3a–3e show the integration of fractional variance in the same five frequency bands as that shown in Figure 1 except for EXP2. The black lines labeled 30, 60, 90, 120, and 150 are the positions of the critical latitude θ_c for five selected wave periods from 30 to 150 days. One notices that these black lines move closer to the equator as compared with their counterparts in the previous experiment in Figure 1. These changes are exactly what one would expect from the dependence of critical latitude on c_1 as expressed by equation (5). The frequency distribution of the peak-spectrum SSH variability (color shaded) also moves closer to the equator and, in fact, matches well with the shift of θ_c distribution. When the value of c_1 is increased, as in EXP3, the distributions of peak-spectrum frequency and θ_c both move coherently to the poles (Figure 4).

We have conducted several additional experiments by changing c_1 and the model results are all consistent with the LIN08 mechanism. The model experiments demonstrated unambiguously that the distribution of

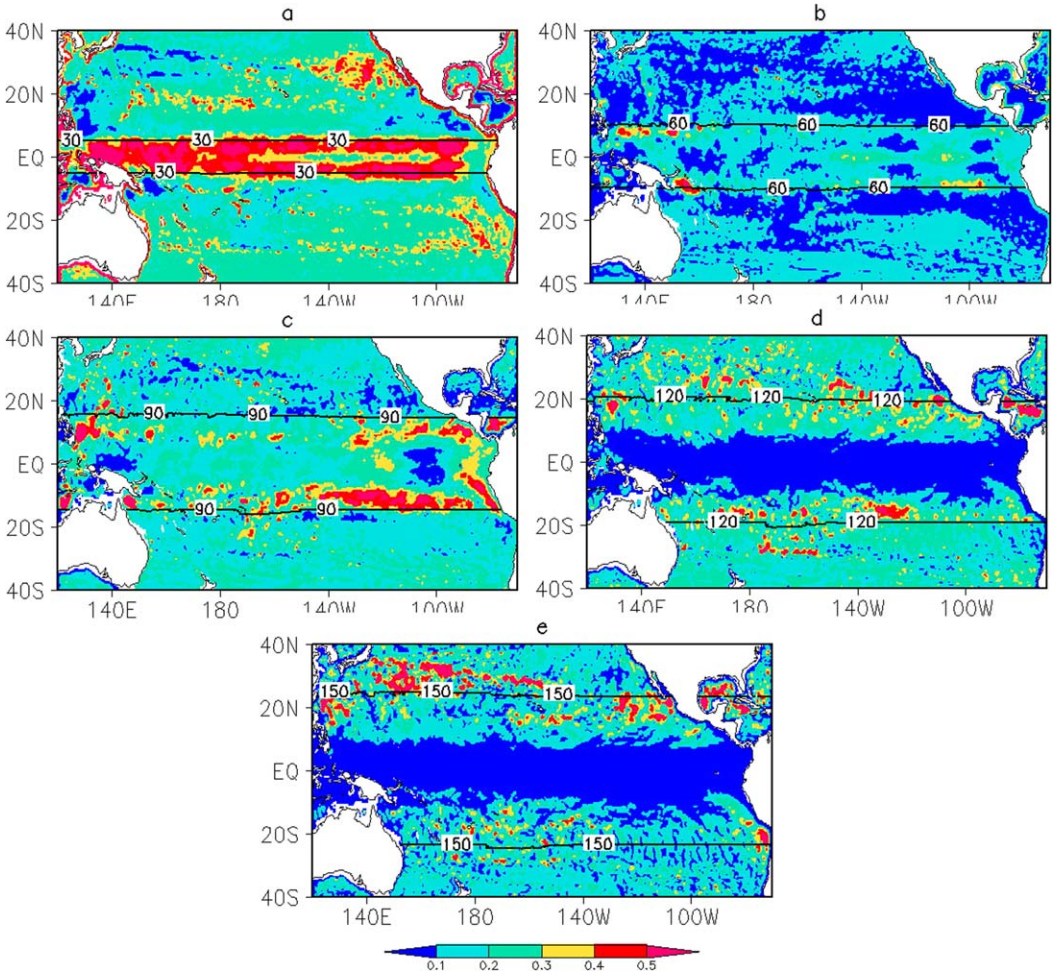

Figure 3. The same as Figure 1 except for EXP2. The density difference between the first and second layers is half, compared to the EXP1, and c_1 is about 2.5 m s^{-1}. The reduction of the deformation radius, c_1/f, leads to a lower critical latitude for a given frequency (compare the black lines here with those in Figure 1). The distribution of peak-spectrum frequencies (color shading) move accordingly toward the equator.

the peak-spectrum SSH variability is determined by the ocean dynamics rather than by being imposed by a dominant frequency in the forcing field (wind stress in the model). An apparently good match between the critical latitudes of Rossby waves and the peak-spectrum SSH variability also indicate that the linear wave theory is a plausible mechanism for explaining the latitudinal dependence of peak-spectrum SSH variability.

Like that in LIN08, our analyses so far have been restricted to area within 40° in latitude and to 150 days in period and focused only on the role of linear Rossby waves. Altimetry data do not have a sufficient resolution to resolve the critical wave length of a baroclinic Rossby wave in high latitudes. But as noted in numerous previous studies, eddies are a dominant feature in SSH observations. Eddies and Rossby waves share some common characteristics. They all tend to move westward. In addition, eddies and Rossby waves have similar zonal phase speeds and frequencies [*Chelton et al.*, 2011; *Early et al.*, 2011]. Does the LIN08 mechanism still apply in subpolar basins or when eddies are considered? In the following, we will examine outputs from an eddy-resolving model, the OFES from Japan's Earth Simulator.

4. OFES Data Analysis

The OFES is based on the Geophysical Fluid Dynamics Laboratory's Modular Ocean Model (MOM3). The model domain covers 75°S–75°N with horizontal grid spacing of 1/10°. A detailed description of the model

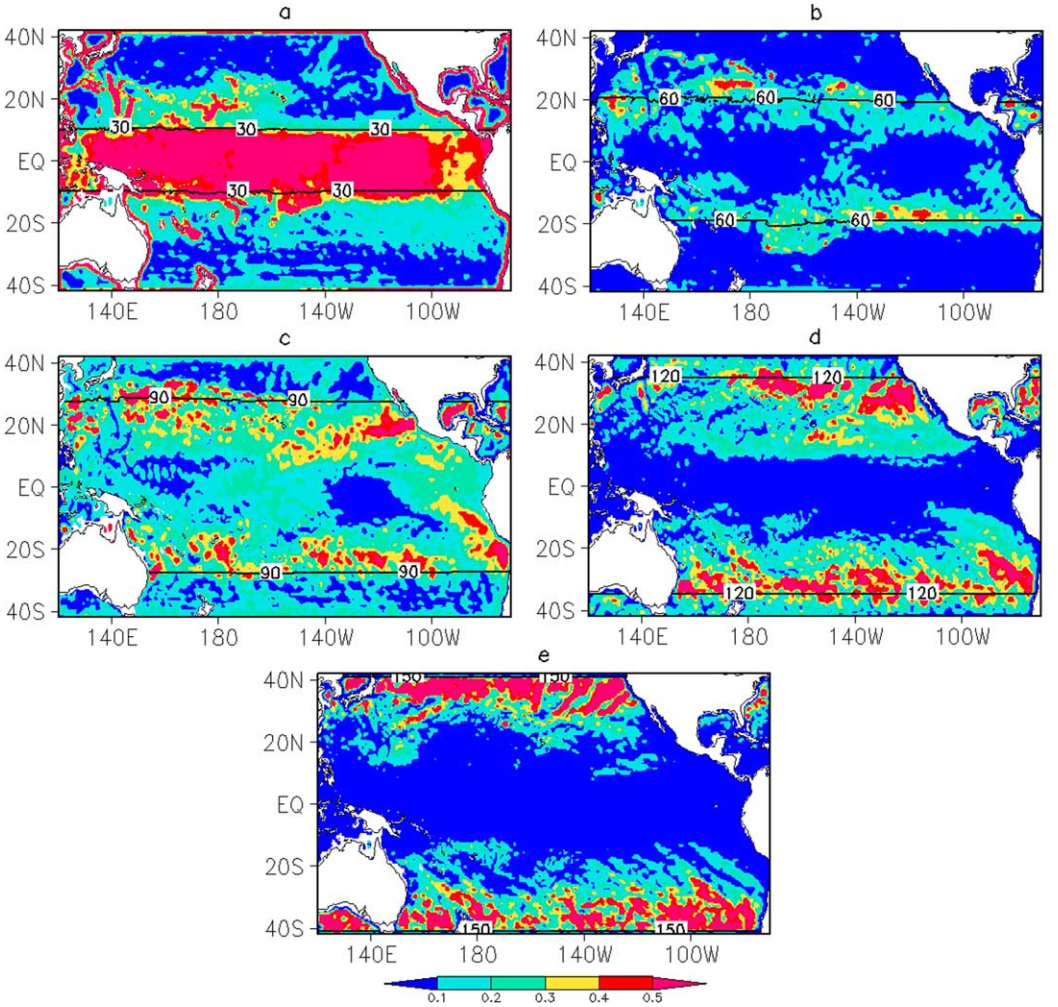

Figure 4. The same as Figure 1 except for EXP3. The density difference between the first and second layer is double compared to the EXP1, and c_1 is about 5.1 m s^{-1}. Opposite to EXP2, the increase of c_1 moves the critical latitude poleward (black lines). The distribution of the model simulated SSH variability changes accordingly (color shading for the distribution of peak-spectrum frequencies). Together with EXP2, this shows that the distribution of the peak-spectrum SSH variability is not imposed locally by the wind stress forcing, but rather is determined by the oceanic dynamics, specifically the stagnant Rossby waves.

formulation was given by *Masumoto et al.* [2004]. Following a 50 year spin-up simulation with a monthly mean climatological forcing, a hindcast simulation from 1950 to 2004 [*Sasaki et al.*, 2004, 2008] was conducted by using a daily mean surface forcing derived from the NCEP/NCAR reanalysis. To compare with the altimetry data, we use the OFES SSH in the period of 1990–2004 with a 3 day interval. The area for this study is from 60°S to 60°N. The climatological temperature and salinity from 1990 to 2004 are also used in our study to calculate the Rossby deformation radius which is needed in the computation of the critical frequency, critical wave length, and critical latitude of zonal stagnant Rossby waves.

We use the FFT to calculate the power spectrum at every grid point. The 15 year OFES output used in this analysis is archived with a 3 day interval with a total of 1826 samples at each grid point. Therefore, the power spectrum is computed over 913 period bands (as listed in Table 1) from as short as 6 days to as long as 15 years.

The spectrum of an oceanic time series is typically red and increases toward a longer period [*Hasselmann*, 1976]. In this study, we are primarily interested in whether the spectrum of SSH variations peak at the critical frequency and also analyze SPD as in section 3. So our analysis is limited to 10 main period bands from 30 to 450 days (Table 1). They represent variability in wave periods of 1, 2, 3, 4, 5, 6, 8, 10, 12, and 15

Table 1. The Period Bands in the FFT Results and the Definition of 10 Main Frequency Bands

	Period Band	
I	Day	Month
913	6	
...	...	
366	14.97	
365	15.01	1
...	...	
112	44.90	
111	45.31	2
...	...	
68	74.39	
67	75.52	3
...	...	
48	106.04	
47	108.35	4
...	...	
38	134.70	
37	138.44	5
...	...	
32	160.77	
31	166.13	6
...	...	
26	199.36	
25	207.67	8
...	...	
20	262.32	
19	276.89	10
18	293.18	
17	311.50	
16	332.27	12
15	356.00	
14	383.38	
13	415.33	15
12	453.09	
11	498.40	
10	547.80	
...	...	
1	5478.00	

months. We should point out here that the main period bands are irregular when we extend our analysis to longer period (longer than 6 months) because the period (frequency) resolution is low in the long period (low frequency) band of FFT results. For a period shorter than 6 months, it is about 30 days in each main period band. But it is 55 days in 8 month period band, 35 days in 10 month period band, 51 days in 12 month period band, and 83 days in 15 month period band. The reason for using such irregular range in the longer period bands is to ensure at least three period bands of FFT results included in each main period band. The critical frequency (period) for a free and linear first baroclinic mode Rossby wave between 60°S and 60°N is usually higher than 2π/(2 years). The cutoff period of 498.4 days chosen in the present study also covers most of the critical periods in the world oceans.

Figure 5 shows the fractional variance for each of the 10 chosen period bands to the total variability (between 15 and 498.4 days) (background color). The black lines indicate the position of the critical latitude θ_c for a period of 30 days (Figure 5a), 60 days (Figure 5b), 90 days (Figure 5c), 120 days (Figure 5d), 150 days (Figure 5e), 180 days (Figure 5f), 240 days (Figure 5g), 300 days (Figure 5h), 360 days (Figure 5i), and 450 days (Figure 5j). The deformation radius c_1/f in (3) is computed by using the hydrographic and bathymetric data from OFES in a procedure described by *Gill* [1982]. The position where the spectrum peaks at each chosen period aligns well with the critical latitude defined by (3) except for the annual cycle (Figure 5i). It is understandable that the ocean has a large response to seasonal cycle even in areas that are away from the critical latitude. It simply shows the dominance of the annual cycle in the forcing fields. For other periods, the spectrum typically peaks within 5° from the critical latitude in the tropical and subtropical basins. The SSH variability within each selected period band usually contributes >30% to the total power spectrum. In high latitudes, however, the frequency that the SSH has the maximum spectrum does not correspond as well to the critical Rossby-wave frequency as it does in low latitudes. First, the zonal band of high peak-spectrum SSH variability is not as sharply defined and has a greater latitudinal spread than that in the low latitudes. Second, the SSH variability within each critical period band contributes less to the total power spectrum, about 20% as compared with 30% in lower latitudes. Third, the SSH variability in the ACC is very energetic near the 1 month period (Figure 5a), which is much shorter than the critical period of the first baroclinic mode Rossby waves in such a high latitude. This latitudinal difference in our analyses appears to be consistent with the results by *Hughes and Williams* [2010] that a linear wave model is suitable for SSH variability only in the low latitudes. Nonlinear eddies play a more prominent role in the high-latitude oceans.

We have applied the two-dimensional FFT (zonal direction and time) to SSH data in each latitudinal band in the Pacific Ocean and then projected the power spectrum into the wave length and period space. A bandpass filter of 20–1600 km in wave length and 30–600 days in period is applied. Figures 6a and 6b are the power spectrum in wavelength-latitude and period-latitude spaces. The solid lines in Figure 6 are the corresponding critical wavelength and period that were calculated by using the hydrography from the OFES output. The white lines in Figure 6 are the wavelength or period that are associated with the maximum SSH variance. The high-spectrum band of the SSH variability is basically centered along the critical wave length

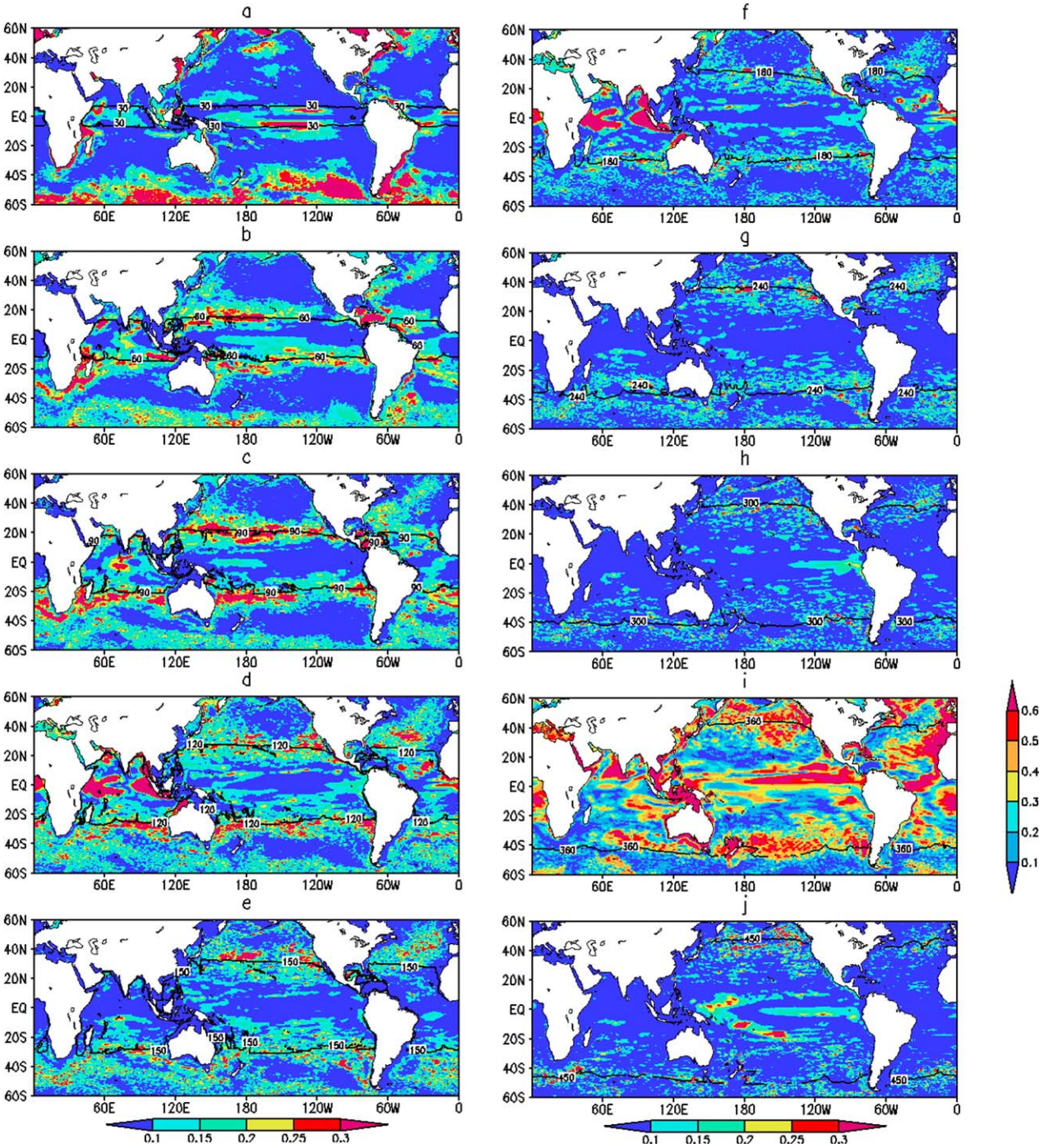

Figure 5. The fractional variance (color shading) between a selected period band and the accumulated one for the period $<$498.4 days. The selected period band is: (a) 1 month, (b) 2 month, (c) 3 month, (d) 4 month, (e) 5 month, (f) 6 month, (g) 8 month, (h) 10 month, (i) 12 month, and (j) 15 month as listed in Table 1. The data used here are 15 year (1990–2004) OFES SSH. Note that there are zonal bands of high-energy spectrum in each period range. The black lines represent the critical latitude θ_c, which is defined by equation (5) and calculated by OFES temperature and salinity, for the following frequencies: (a) $2\pi/30$ days, (b) $2\pi/60$ days, (c) $2\pi/90$ days, (d) $2\pi/120$ days, (e) $2\pi/150$ days, (f) $2\pi/180$ days, (g) $2\pi/240$ days, (h) $2\pi/300$ days, (i) $2\pi/360$ days, and (j) $2\pi/450$ days. The 12 month period fractional variance uses a specific color bar in Figure 5i. It is obvious that the periods of energetic SSH spectrum (color) are near the critical periods of Rossby waves (black lines).

L_c in Figure 6a. The wavelength associated with the peak-spectrum variability decreases poleward as the critical wavelength of linear Rossby waves does. Our results are similar to that shown by *Stammer* [1997] who found the peak-spectrum along-track length scales have a good correlation with the critical wave

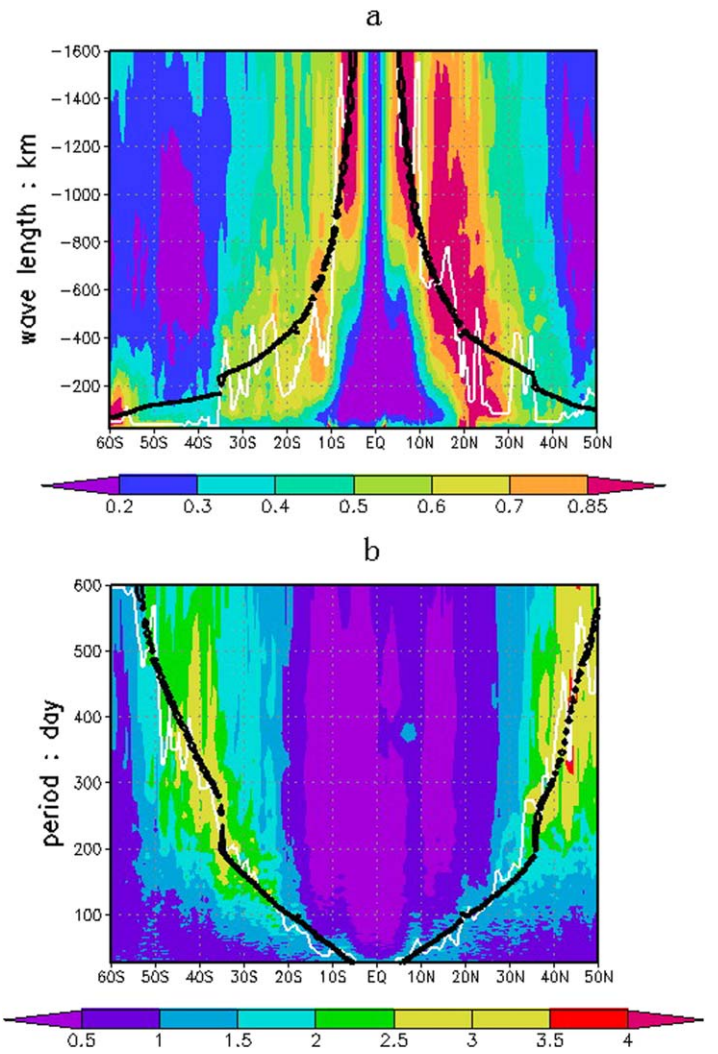

Figure 6. (a) The wave length-latitude energy spectrum and (b) period-latitude energy spectrum from OFES SSH data (color shading). The black lines are the theoretically expected critical wave length and the critical period (computed by using potential density from OFES). The white lines are the most energetic wave length and the period. We conduct a band pass of 20–1600 km in wave length and a period of 30–600 days.

lengths, while the former is much longer than the latter in the extratropical oceans, with a factor of 3 larger in high latitudes (Figure 25 in his paper). But the peak-spectrum wavelengths of the SSH variability are even closer to the critical wave lengths in our results. It is not realistic to expect that these two wavelengths, i.e., the data-derived peak-spectrum wavelength and the theoretically defined critical wavelength, to match exactly. Processes other than linear Rossby waves are also at play in the ocean. In fact, one can notice some differences between the black (theory) and white (data) lines in Figure 6. Along 10°N and 10°S, the peak-spectrum wave length is longer than the critical wave length with a difference of $>$30%, while in 20° bands the peak-spectrum wavelength seems shorter than the critical wavelength. The differences between these two wavelengths in the high latitudes are even more pronounced. But overall the agreement is considerable. The agreement between the peak-spectrum period and the critical period is better than that in the comparison in the wavelength domain. The white line of the peak-spectrum period is nearly perfectly along the black line of the critical wave period $2\pi/\omega_c$ in Figure 6b. The difference between these two curves is usually $<$20%, and the larger deviations are also located in high latitudes.

The above analysis supports the findings of LIN08 that the power spectrum of the SSH variability tends to peak at the critical latitude and frequency of linear Rossby waves in low and moderate latitudes. The significance of the critical latitude/frequency of linear Rossby waves in the SSH spectrum, however, fades in high latitudes. There are several possible causes for this diversion, including but not limited to: (1) a larger contribution from the barotropic or second and higher baroclinic modes to the SSH variability; (2) contributions to SSH variability from processes other than linear and free Rossby waves; (3) strong current-wave or wave-wave interactions; (4) an increasing dominance of mesoscale eddies; and (5) topographic effects. For example, the dominant 1 month period variability in the ACC region as shown in Figure 5a could be attributed to eddies. The Southern Ocean is an area where the linear planetary Rossby wave theory may have reached its limitation as eddies and/or topographic waves play a more active role and interactions with a strong ACC cannot be ignored [e.g., *Hughes et al.*, 1998; *Fu*, 2009]. Some previous studies also suggested that large variability near the 30 day period is associated with barotropic waves [*Fukumori et al.*, 1998; *Webb and de Cuevas*, 2002, 2003].

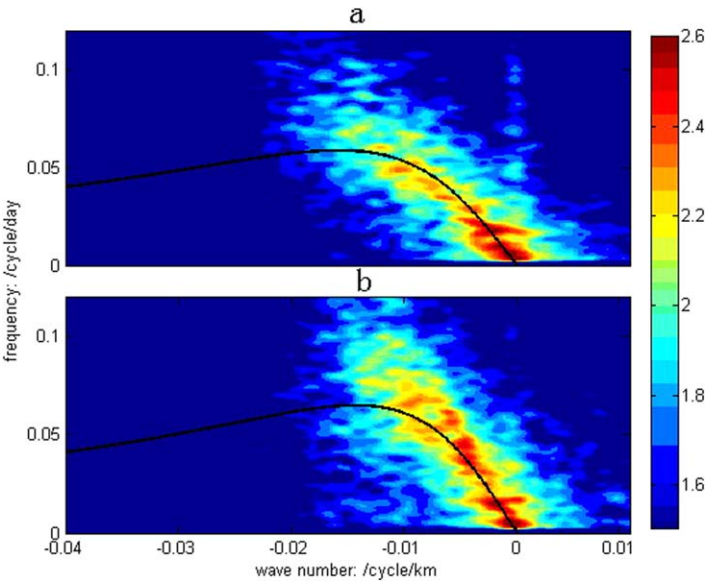

Figure 7. Zonal wave number-frequency spectrum along 20°N in the Pacific Ocean (a) spectrum from 160°W to 115°W and (b) spectrum from 135°E to 180°E.

Both linear model experiments and OFES data analyses indicate linear wave theory may explain the peak-spectrum SSH variance near critical frequency in low latitude and midlatitude. But other processes, such as eddies, are clearly important too. For example, eddies that are generated by the shear instability of North Equatorial Current and Subtropical Counter Current has a dominant period of 100 days [*Qiu*, 1999], which is near the critical period of the first baroclinic mode Rossby waves at 20°N. Because eddies and waves have different dispersion relations, one can separate them by using both frequency and wave number. Here is an example. We calculate the zonal wave number-frequency spectrum in two bands along 20°N in the Pacific Ocean. Figure 7a is the spectrum from 160°W to 115°W, in which eddies' activity is relatively low. Figure 7b is the spectrum from 135°E to 180°E, in which eddies are very active as shown by *Qiu* [1999]. The black lines in Figure 7 are the curve of dispersion relation from the first baroclinic mode Rossby waves calculated by using OFES density data in each zonal band. In the eastern Pacific Ocean along 20°N, the distribution of energy spectrum is very well along the black line, indicating the linear wave dynamics indeed dominates the SSH variability in this region. In the western Pacific Ocean along 20°N, the distribution of energy spectrum is deviated from the dispersion curve near the large wave number or high frequency. This is consistent with recent studies [*Chelton et al*., 2011; *Early et al*., 2011] that nonlinear eddies have a phase speed similar to the nondispersive long waves, even for mesoscale features. But the zonal phase speed for the zero zonal group velocity waves is actually lower (by half) than the zonal phase speed for nondispersive long waves. So the SSH variability determined by linear wave would have a shorter wave length than that by eddies near the critical frequency. This is clearly shown in Figure 7 and can partly explain why the latitudinal dependence of peak-spectrum SSH variability has a better correlation with the critical period than with the critical wave length.

Next, we will use the dispersion relation as a criterion to compare the contribution from linear waves and nonlinear eddies to the total peak-spectrum SSH variability near the critical frequency. Our hypothesis is based on the fact that the linear and free waves follow the dispersion relation. First, we calculate energy spectrum by using FFT at each grid point in OFES SSH data in the Pacific Ocean from 50°S to 50°N. Second, a band filter with the window of 0.8–1.2 critical periods is applied and the time filtered SSH variability includes contributions from both linear waves and nonlinear eddies near the critical frequency. Third, a band filter with the window of 0.8–1.2 zonal critical wavelengths is further applied in each grid in the zonal direction and this spatial filtered SSH variability would only include linear waves. The ratio of linear waves energy (after two filters) and combined wave and eddies energy (after the first filter) in the Pacific Ocean is shown in Figure 8, which indicates the contribution from linear waves to the total SSH variability near the critical frequency. Due to the spatial band filter, there is no data near the boundary within the distance less than half critical wave length. The overall pattern in Figure 8 shows that linear waves are dominant in SSH variability in the tropical and subtropical regions, especially in the Eastern Pacific Ocean. In the regions with more active eddies like the Subtropical Counter Current [*Qiu*, 1999; *Qiu and Chen*, 2004] and the Coral Sea [*Qiu et al*., 2008], linear waves can only explain $<$50% of SSH variability near the critical frequency. To the higher latitudes, the ratio that can be explained by linear waves decreases to $<$30%. Figure 8 is also comparable with the results of *Chelton et al*. [2007] who showed that eddies are more active in the western Pacific

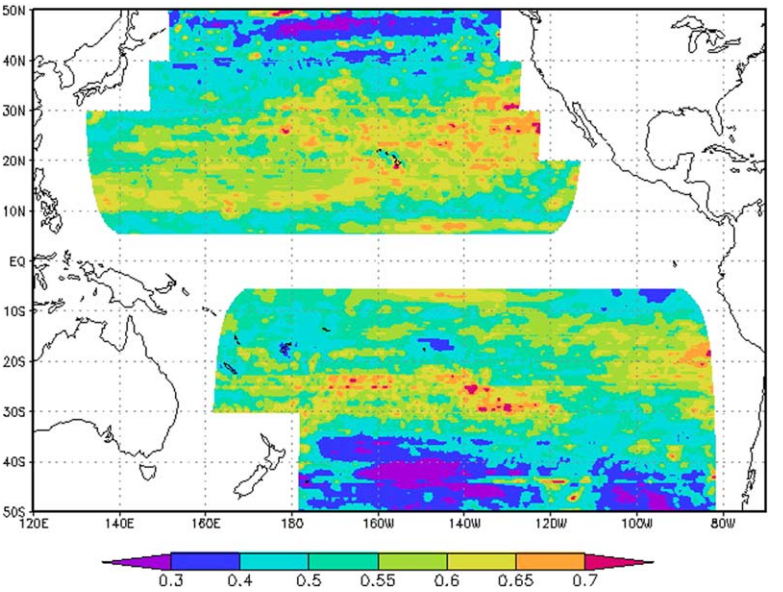

Figure 8. The ratio between waves energy only (band filtered both by critical period and wave length from 0.8 to 1.2) and total energy (waves and eddies energy, band filtered only by critical period from 0.8 to 1.2) near critical frequency.

Ocean and in high latitudes. We have used different windows in filter process and the ratio pattern is similar to Figure 8, with only a slight change of value.

5. Summary and Discussion

In this paper, we have further studied the mechanism of latitudinal dependence of peak-spectrum SSH variability by extending our analyses to the OFES output, which has a higher resolution than the altimetry data to better resolve the critical wavelength, and by using a linear RG model. The purpose of this study is to test the dynamical consistency of LIN08s hypothesis with the dispersion relation of linear Rossby waves and to identify areas where other mechanisms such as eddies become more important.

There are two specific objectives for this study. The first one is to test the dynamical consistency with the theory by using a linear wave model. The single most important dynamical parameter in the dispersion relation is the deformation radius. The critical latitude moves poleward and the critical frequency increases when the deformation radius increases. If the LIN08 mechanism holds, one expects that the latitudinal position of the peak-spectrum SSH variations at a chosen frequency moves poleward when the deformation radius increases even under the same atmospheric forcing. The results from three selected experiments are shown in this study. When the deformation radius is altered, the model results and the sense of the changes all suggest that Rossby waves with zero group velocity are indeed responsible for the distribution of the peak-spectrum SSH variability in the tropical and subtropical oceans.

The second objective is to extend LIN08s analysis to higher latitudes where altimetry data are too coarse to resolve baroclinic waves at their critical frequency. Applying the same spectra analysis to a higher resolution OFES data yields results similar to that from using altimetry data in the tropical and subtropical oceans. But in high latitudes, we have identified a number of discrepancies between data and linear wave theory. This indicates that linear waves are insufficient to account for the SSH variability in high latitudes.

Chelton et al. [2007, 2011] showed that most of mesoscale SSH variability over much of the World Ocean is accounted for by eddies with a typical amplitude of 5–25 cm and diameter of 100–200 km. They were interpreted as nonlinear vortices [*McWilliams and Flierl*, 1979] because of their small excursions in the meridional direction. This is different from these early studies that the SSH variability is mainly interpreted as Rossby

waves [*Chelton and Schlax*, 1996]. In this study, we have examined whether the peak-spectrum SSH variability is dominated by eddies rather than linear Rossby waves. Due to the similar properties between the nonlinear eddies and waves, it is difficult to separate linear waves from eddies near the critical frequency. We designed and applied a filter in both space and time to the OFES SSH data, and showed that the linear wave theory remains valid in explaining the latitudinal dependence of peak-spectrum SSH variability in the tropical and subtropical oceans, especially in the Eastern Pacific Ocean. On the other hand, eddies contribute more in the western Pacific Ocean and in high latitudes.

Acknowledgments
We have benefited from talking with Joe Pedlosky, Terry Joyce, and John Toole. The OFES simulation was conducted on the Earth Simulator under the support of JAMSTEC. This work was supported by the China's National Basic Research Priorities Programmer (2013CB956202), Strategic Priority Research Program of the Chinese Academy of Sciences (XDA11010103), the Natural Science Foundation of China (41222037 and 41221063), the project of Global Change and Air-Sea interaction (GASI-03-01-01–02), the Ministry of Education's 111 Project (B07036), the National Natural Science Foundation of Shandong (JQ201111), and the National Special Research Fund for Non-Profit Marine Sector (201205018). J. Y. is supported by US NSF (OCE 0927017 and OCE 1028739).

References

Chelton, D. B., and M. G. Schlax (1996), Global observations of oceanic Rossby waves, *Science*, *272*, 234–238.
Chelton, D. B., M. G. Schlax, R. M. Samelson, and R. A. deSzoeke (2007), Global observations of large oceanic eddies, *Geophys. Res. Lett.*, *34*, L15606, doi:10.1029/2007GL030812.
Chelton, D. B., M. G. Schlax, and R. M. Samelson (2011), Global observations of nonlinear mesoscale eddies, *Prog. Oceanogr.*, *91*, 167–216, doi:10.1016/j.pocean.2011.01.002.
Chen, H. Y., F. L. Qiao, and Y. G. Wang (2003), Zonal propagation velocity distribution characteristics of oceanic Rossby waves, *Adv. Mar. Sci.*, *21*, 387–392.
Cooley, J. W., and J. W. Tukey (1965), An algorithm for the machine calculation of complex Fourier series, *Math. Comput.*, *19*, 297–301.
Early, J. J., R. M. Samelson, and D. B. Chelton (2011), The evolution and propagation of quasigeostrophic ocean eddies, *J. Phys. Oceanogr.*, *41*, 1535–1555, doi:10.1175/2011JPO4601.1.
Flierl, G. R. (1978), Models of vertical structure and the calibration of two-layer models, *Dyn. Atmos. Oceans*, *2*, 341–381.
Fu, L.-L. (2009), Pattern and velocity of propagation of the global ocean eddy variability, *J. Geophys. Res.*, *114*, C11017, doi:10.1029/2009JC005349.
Fu, L.-L., and D. B. Chelton (2001), Large-scale ocean circulation, in *Satellite Altimetry and Earth Sciences: A Handbook for Techniques and Applications*, edited by L.-L. Fu and A. Cazenave, pp. 133–169, Academic, London, U. K.
Fukumori, I., R. Raghunath, and L.-L. Fu (1998), Nature of global large-scale sea level variability in relation to atmospheric forcing: A modeling study, *J. Geophys. Res.*, *103*, 5493–5512, doi:10.1029/97JC02907.
Gill, A. E. (1982), *Atmosphere–Ocean Dynamics*, 662 pp., Academic, London, U. K.
Glazman, R. E., and P. B. Weichman (2005), Meridional component of oceanic Rossby wave propagation, *Dyn. Atoms. Oceans*, *38*, 173–193.
Hasselmann, K. (1976), Stochastic climate models Part I. Theory, *Tellus*, *28*, 473–485.
Hu, R. J., and Q. Y. Liu (2002), Annual and intraseasonal variations in sea surface height over the topic Pacific, *J. Oceanol. Limnol.*, *33*, 303–313.
Hughes, C. W., and S. D. P. Williams (2010), The importance of spatial variations in spectral shape for assessing the significance of trends, *J. Geophys. Res.*, *115*, C10048, doi:10.1029/2010JC006102.
Hughes, C. W., M. S. Jones, and S. Carnochan (1998), Use of transient features to identify eastward currents in the Southern Ocean, *J. Geophys. Res.*, *103*, 2929–2944.
Lighthill, M. J. (1969), Dynamic response of the Indian Ocean to onset of the Southwest Monsoon, *Philos. Trans. R. Soc. London A*, *265*, 45–92.
Lin, X. P., D. W. Wu, and J. Lan (2004), The intrusion and influence of intraseasonal long Rossby waves in the East China Sea, *J. Hydrodyn., Ser. B*, *16*, 621–631.
Lin, X. P., J. Yang, D. Wu, and P. Zhai (2008), Explaining the global distribution of peak-spectrum variability of sea surface height, *Geophys. Res. Lett.*, *35*, L14602, doi:10.1029/2008GL034312.
Liu, Q. Y., and Q. Wang (1999), Spatial distribution of the sea surface height intraseasonal oscillation in the tropical Pacific, *J. Ocean Univ. Qingdao*, *29*(4), 549–555.
Liu, W. T. (2002), Progress in scatterometer application, *J. Oceanogr.*, *58*, 121–136.
Masumoto, Y., et al. (2004), A fifty-year eddy-resolving simulation of the world ocean—Preliminary outcomes of OFES (OGCM for the Earth Simulator), *J. Earth Simulator*, *1*, 35–56.
McWilliams, J. C., and G. R. Flierl (1979), On the evolution of isolated, nonlinear vortices, *J. Phys. Oceanogr.*, *9*, 1155–1182.
Mitchum, G. T. (1995), The source of 90-day oscillations at Wake Island, *J. Geophys. Res.*, *100*(C2), 2459–2475.
Pan, A. J., Q. Y. Liu, R. J. Hu, and S. X. Wang (2002), Quasi 90-day oscillation of the current in the area of subtropical countercurrent in the North Pacific, *J. Ocean Univ. Qingdao*, *32*, 18–24.
Pedlosky, J. (1987), *Geophysical Fluid Dynamics*, 710 pp., Springer, New York.
Polito, P. S., and P. Cornillon (1997), Long baroclinic Rossby waves detected by TOPEX/POSEIDON, *J. Geophys. Res.*, *102*(C2), 3215–3235, doi:10.1029/96JC03349.
Polito, P. S., and W. T. Liu (2003), Global characterization of Rossby waves at several spectral bands, *J. Geophys. Res.*, *108*(C1), 3018, doi:10.1029/2000JC000607.
Qiao, F. L., E. Tal, and Y. L. Yuan (2004), Zonal distribution features of high frequency planetary waves in the oceans derived from satellite altimeter data, *Acta Oceanol. Sin.*, *23*(1), 91–96.
Qiu, B. (1999), Seasonal eddy field modulation of the North Pacific Subtropical Countercurrent: TOPEX/Poseidon observations and theory, *J. Phys. Oceanogr.*, *29*, 2471–2486.
Qiu, B., and S. M. Chen (2004), Seasonal modulations in the eddy field of the South Pacific Ocean, *J. Phys. Oceanogr.*, *29*, 2471–2486.
Qiu, B., W. Miao, and P. Muller (1997), Propagation and decay of forced and free baroclinic Rossby waves in off-equatorial oceans, *J. Phys. Oceanogr.*, *27*, 2405–2417.
Qiu, B., R. B. Scott, and S. M. Chen (2008), Length scales of eddy generation and nonlinear evolution of the seasonally modulated South Pacific Subtropical Countercurrent, *J. Phys. Oceanogr.*, *38*, 1525–1528.
Sasaki, H., Y. Sasai, S. Kawahara, M. Furuichi, F. Araki, A. Ishida, Y. Yamanaka, Y. Masumoto, and H. Sakuma (2004), A series of eddy-resolving ocean simulations in the world ocean: OFES (OGCM for the Earth Simulator) project, *OCEAN'04*, *3*, 1535–1541.
Sasaki, H., M. Nonaka, Y. Masumoto, Y. Sasai, H. Uehara, and H. Sakuma (2008), An eddy-resolving hindcast simulation of the quasi-global ocean from 1950 to 2003 on the Earth Simulator, in *High Resolution Numerical Modelling of the Atmosphere and Ocean*, edited by W. Ohfuchi and K. Hamilton, pp. 157–186, Springer, New York.
Stammer, D. (1997), Global characteristics of ocean variability estimated from regional TOPEX/POSEIDON altimeter measurements, *J. Phys. Oceanogr.*, *27*, 1743–1769.

Webb, D. J., and B. A. de Cuevas (2002), An ocean resonance in the Indian sector of the Southern Ocean, *Geophys. Res. Lett.*, *29*(14), 1664, doi:10.1029/2002GL015270.

Webb, D. J., and B. A. de Cuevas (2003), The region of large seasurface height variability in the Southeast Pacific Ocean, *J. Phys. Oceanogr.*, *33*, 1044–1056.

White, W. B., C. Yi, and C. K. Tai (1998), Coupling of biennial oceanic Rossby waves with the overlying atmosphere in the Pacific basin, *J. Phys. Oceanogr.*, *28*, 1236–1251.

Yang, J., and T. Joyce (2006), Local and equatorial forcing of seasonal variations of the North Equatorial Countercurrent in the Atlantic Ocean, *J. Phys. Oceanogr.*, *36*, 238–254.

Zhang, D. X., T. N. Lee, W. E. Johns, C. T. Liu, and R. Zantopp (2001), The Kuroshio east of Taiwan: Modes of variability and relationship to interior ocean mesoscale eddies, *J. Phys. Oceanogr.*, *31*, 1054–1074.